Improved detection of sulphur dioxide in volcanic plumes using satellite-based hyperspectral infrared measurements: Application to the Eyjafjallajökull 2010 eruption

J. C. Walker,[1] E. Carboni,[1] A. Dudhia,[1] and R. G. Grainger[1]

Received 31 August 2011; revised 31 December 2011; accepted 6 January 2012; published 14 March 2012.

[1] The explosive phase of the eruption of the Eyjafjallajökull volcano in Iceland beginning on 14 April 2010 caused extensive disruption to aviation in Europe with serious social and economic consequences. Despite its impact, the explosive phase was modest in size and the amount of sulphur dioxide (SO_2) released was low. The potential of hyperspectral thermal infrared measurements to discriminate emissions from similar events by measuring SO_2 is examined using the Infrared Atmospheric Sounding Interferometer (IASI) on board MetOp-A. The transported plume in the initial stages of the explosive phase contained low amounts of SO_2 at low altitude which placed it at the detection limit of space-based sensors used to monitor the volcanic threat to aviation using current methods. A recently developed technique for the fast retrieval of SO_2 from IASI is applied in the context of the Eyjafjallajökull eruption to show that IASI is easily capable of sensing the SO_2 in the plume at this stage where existing methods fail. The fast SO_2 retrieval is calibrated against a fully quantitative optimal estimation retrieval of SO_2 total column amount and plume altitude to derive the detection limit for the plume on 15 April 2010. An estimate of the general detection limit for the instrument is placed conservatively at 0.3 Dobson Units (DU) which is an order of magnitude lower than previously thought.

Citation: Walker, J. C., E. Carboni, A. Dudhia, and R. G. Grainger (2012), Improved detection of sulphur dioxide in volcanic plumes using satellite-based hyperspectral infrared measurements: Application to the Eyjafjallajökull 2010 eruption, *J. Geophys. Res.*, *117*, D00U16, doi:10.1029/2011JD016810.

1. Introduction

[2] A modest explosive eruption of the Eyjafjallajökull volcano in Iceland (63.63°N, 19.62°W, 1666 m above sea level [asl]) began on 14 April 2010 after a preceding effusive phase and continued with varying intensity until 24 May 2010. A plume of gas and fine-grained volcanic ash was ejected to altitudes of almost 8 km asl [*Stohl et al.*, 2011; *Gudmundsson et al.*, 2010] and transported south-east towards Europe by the prevailing meteorological conditions, resulting in the closure of large areas of European airspace on several occasions during this period with serious social and economic impacts. The threat posed to air-traffic by an Icelandic eruption had been noted previously [*Prata*, 2009], and there is the potential for further disruption across Europe or the North Atlantic Tracks, as evidenced by the November 2004 eruption of the Grímsvötn volcano [*Witham et al.*, 2007], which caused some grounding of European air-traffic, and further eruptions at this volcano in May 2011 [*Showstack*, 2011]. The main hazard to aircraft is the fine-grained rock, mineral fragments and glass shards within the ash plume that can cause engine damage or even engine failure, as well as abrasion of forward facing surfaces and reduced visibility [e.g., *Carn et al.*, 2009; *Guffanti et al.*, 2010]. Satellite measurements are essential for effective hazard mitigation because of the remoteness of many volcanoes, the sporadic nature of the eruptions, and the rapid spread of emissions [*Prata*, 2009]. The Eyjafjallajökull eruption was rated at 4 on the Volcanic Explosivity Index (VEI) (http://www.volcano.si.edu/world/volcano.cfm?vnum=1702-02=&volpage=erupt). Globally, explosive volcanic eruptions of this size are not uncommon and are expected every few years on average [*Simkin*, 1993]. The satellite-based detection of small, frequent events is essential to reduce the hazard posed to aviation [*Carn et al.*, 2009; *Miller and Casadevall*, 2000].

[3] Gathering information about volcanic ash clouds to assess the possible hazard to aviation is the official task of the Volcanic Ash Advisory Centers (VAAC's) [*International Civil Aviation Organization* (*ICAO*), 2007; *van Geffen et al.*, 2009]. These centers have the capability to detect, track and forecast the movement of volcanic ash. Information about the current and predicted extent of the volcanic ash cloud and the flight levels affected within their area of responsibility is forwarded to the appropriate bodies to be used to assist operators in the flight planning stage [*ICAO*, 2007]. Reports and forecasts of the ash distribution are provided by

[1]Atmospheric, Oceanic and Planetary Physics, Clarendon Laboratory, University of Oxford, Oxford, UK.

0148-0227/12/2011JD016810

modeling the injection and transport of ash using atmospheric dispersion models such as the Met Office Numerical Atmospheric dispersion Modeling Environment (NAME) [*Jones et al.*, 2007]. Satellite-based infrared and UV-VIS instruments are used to monitor the occurrence of volcanic eruptions and to help visualize the extent and trajectory of the volcanic plumes. It has now been demonstrated that improvements in the quantitative prediction of the fate of volcanic emissions can be obtained by assimilating satellite measurements into ash dispersion models [*Stohl et al.*, 2011], which has become important since ash concentration thresholds for safe flight were introduced in the region affected by Eyjafjalljökull in place of a blanket ban following the extensive disruption caused by this event [*ICAO*, 2010]. While existing methods work very effectively, further developments in near-real-time monitoring are required, and new algorithms and instruments for the detection of volcanic emissions are needed, including methods which are able to detect low altitude plumes from smaller volcanic episodes below the current detection limit [*Thomas and Watson*, 2010].

[4] There are difficulties in relying on satellite measurements of volcanic ash alone to track volcanic plumes as most methods are significantly affected by the ice and water content of the plume. This is likely to have hindered the ash detection from the explosive phase of the Eyjafjallajökull eruption which was initially sub-glacial [*Thomas and Prata*, 2011]. However, using hyperspectral infrared measurements to correlate the spectral shape of the ash plume against the spectral signatures from other eruptions can allow for better discrimination [*Clarisse et al.*, 2010]. Instead of measuring ash, it is often more straightforward to measure SO_2 which is emitted from all major eruptions and can be used as a proxy for ash [*Carn et al.*, 2009]. The gas is easier to detect unambiguously and can be used for the long-range tracking of emissions [*Carn et al.*, 2009; *Karagulian et al.*, 2010]. Comparisons of satellite measurements of the volcanic ash and SO_2 emitted from Eyjafjallajökull indicate that the gas and aerosol plumes were mostly collocated although there were a number of instances where separation occurred due to the more rapid settling of ash compared to SO_2, where in the presence of windshear, ash and SO_2 then follow different trajectories. Under these circumstances, SO_2 can no longer be used as a proxy for ash. It was also noted, however, that in some cases SO_2 that had separated from the main ash cloud could be indicative of the presence of very fine-grained ash, which could pose a hazard and might otherwise not be detected [*Thomas and Prata*, 2011]. As well as being a proxy for volcanic ash, which is the main hazard to aviation, volcanic gases, in particular SO_2, may in themselves pose a risk to aircraft [*Prata and Tupper*, 2009; *Prata*, 2009; *Carn et al.*, 2009]. Long term exposure to SO_2 and its oxidation product sulphuric acid (sulphate aerosol) causes the crazing of acrylic windows and the fading of paint, and has been known to cause the accumulation of sulphate deposits in engine cooling holes which resulted in an engine overheating [*Casadevall et al.*, 1996]. The cumulative effects of repeated exposure to SO_2 is a concern, especially given that diffuse clouds of SO_2 and undetected fine-grained ash can occupy the jet streams which are used by airliners to speed transit. Detection methods need to be as sensitive as possible to see this [*Carn et al.*, 2009].

[5] The first instrument which was able to measure SO_2 from space was the Total Ozone Mapping Spectrometer (TOMS) UV instrument which started to provide data in 1979 and can track SO_2 from very large eruptions. Today, several UV and infrared sensors are able to detect and quantify volcanic SO_2 from space with enough sensitivity for the long-range tracking of emissions [*Prata*, 2009]. To help monitor the volcanic threat to aviation, alert services based on measuring SO_2 are in operation based in Europe and elsewhere which aim to provide information to the relevant authorities who monitor the hazard posed to aviation by volcanic plumes. In Europe, the Support to Aviation Control Service (SACS) provides information to the VAAC's including the London VAAC based at the Met Office, UK, which is responsible for the North Atlantic including the area surrounding Iceland. The scheme has operated very successfully focusing on the timely delivery of SO_2 data from satellite instruments for the monitoring of the occurrence and extension of volcanic eruptions and plumes [*van der A et al.*, 2010].

[6] The system uses state-of-the-art near-real-time SO_2 retrievals from three polar-orbiting UV-VIS instruments: the Global Ozone Monitoring Experiment-2 (GOME-2) on board MetOp-A, the Ozone Monitoring Instrument (OMI) on board EOS-Aura, and the SCanning Imaging Absorption spectroMeter for Atmospheric CartograpHY (SCIAMACHY) on board the ENVIronmental SATellite (ENVISAT). Near-real-time retrievals of SO_2 from GOME-2, which measures backscattered UV-VIS radiation, are performed using a Differential Optical Absorption Spectroscopy (DOAS) type algorithm [*Platt*, 1994; *Valks and Loyola*, 2008; *Rix et al.*, 2008]. Near-real-time retrievals of SO_2 are performed from the OMI instrument using a DOAS type retrieval employing a Band Residual Difference algorithm [*Krotkov et al.*, 2006]. Near-real-time retrievals of SO_2 are performed from SCIAMACHY in the nadir view using a DOAS algorithm [*Platt*, 1994; *Lee et al.*, 2008]. The techniques are implemented for a given altitude of the plume. As this information is generally not known, the SO_2 column product is provided in the form of SO_2 total column loadings conditional on 3 atmospheric layers: planetary boundary layer (for anthropogenic activities or passive degassing conditions), middle troposphere (for effusive eruptions or passive degassing of high volcanoes) and lower stratosphere (explosive eruptions). The error made by assuming a wrong SO_2 altitude is considered as one of the largest errors on the SO_2 columns supplied [*Theys et al.*, 2011]. The SO_2 vertical column product from OMI, GOME-2 and SCIAMACHY for lower stratospheric plumes for the 15 April 2010 in the region of Eyjafjallajökull is shown in Figure 1.

[7] Near-real-time measurements of SO_2 from the infrared instruments IASI on board MetOp-A and the Atmospheric Infrared Sounder (AIRS) on board Aqua are now fully integrated in the SACS system. The IASI measurements are based on measuring the brightness temperature difference (BTD) between two channels in the SO_2 ν_3 vibrational band located in the thermal infrared at 1371.50 and 1371.75 cm^{-1} and two background channels at 1407.25 and 1408.75 cm^{-1} outside the SO_2 band as described by *Clarisse et al.* [2008]. Similarly, the AIRS measurements are used to determine the presence of SO_2 taking the difference in brightness temperature between a small number of channels in the SO_2 ν_3 band

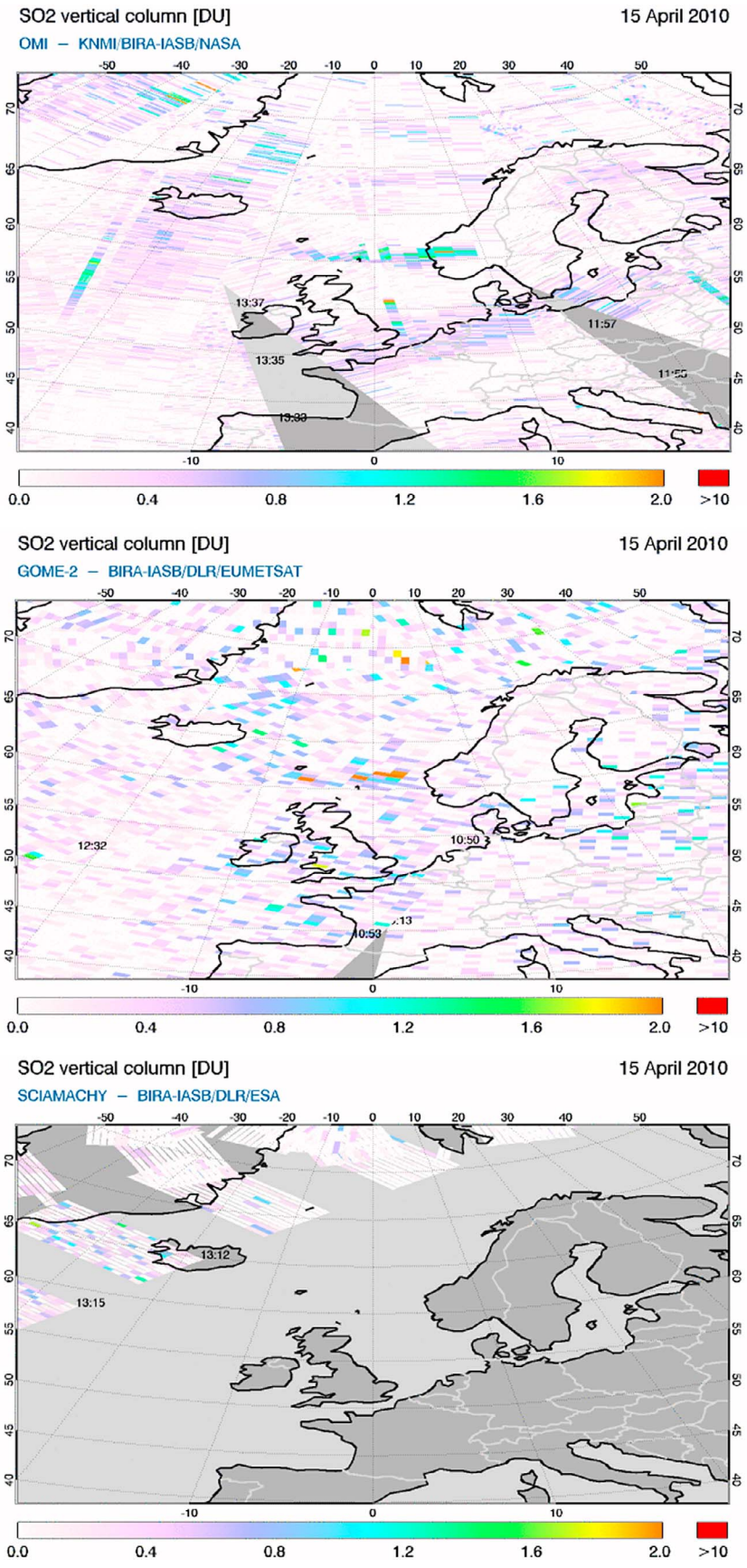
SO2 vertical column [DU]
15 April 2010
OMI – KNMI/BIRA-IASB/NASA
13:37
13:35
13:33
11:57
11:55
0.0 0.4 0.8 1.2 1.6 2.0 >10
SO2 vertical column [DU]
15 April 2010
GOME-2 – BIRA-IASB/DLR/EUMETSAT
12:32
10:50
10:53
0.0 0.4 0.8 1.2 1.6 2.0 >10
SO2 vertical column [DU]
15 April 2010
SCIAMACHY – BIRA-IASB/DLR/ESA
13:12
13:15
0.0 0.4 0.8 1.2 1.6 2.0 >10

Figure 1

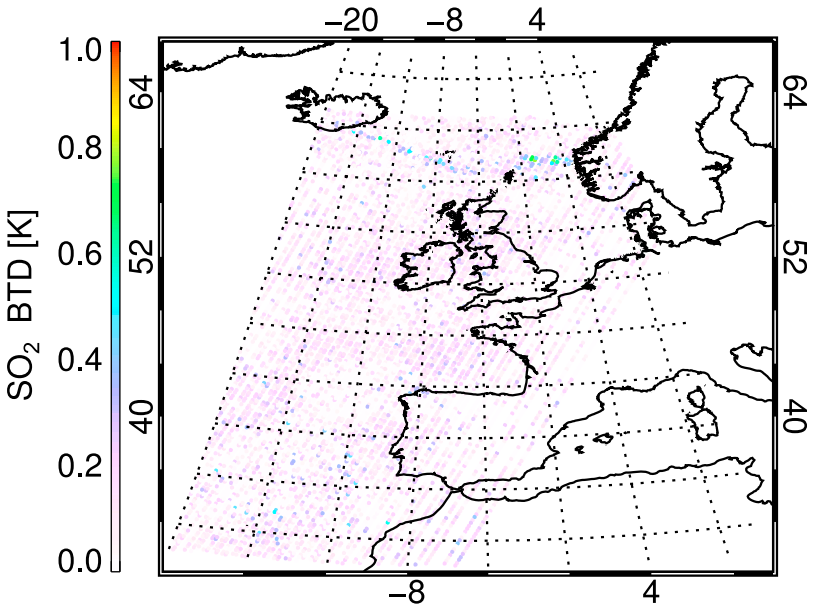

Figure 2. The plume of SO_2 detected from IASI using the BTD method for the morning overpass of 15 April 2010 at 10:48 UTC as the plume drifted toward Scandinavia.

and the spectral baseline [*Theys et al.*, 2011]. Details about SACS can be found on the Web site http://sacs.aeronomie.be/. In the US, similar alert systems are also in place using a combination of UV and thermal infrared instruments. The National Oceanic and Atmospheric Administration (NOAA) SO_2 alert service can be accessed at http://satepsanone.nesdis.noaa.gov/pub/OMI/OMISO2/index.html where links can be found to the OMI SO_2 product and the SO_2 flag using AIRS measurements.

[8] There are several distinct advantages in using infrared measurements for aviation hazard avoidance. The first is that measurements using the ν_3 band are largely insensitive to SO_2 below around 3 km due to strong interference from water vapor which creates a natural filter for emissions that are too low to intersect flight paths [*Prata and Bernado*, 2007]. Infrared sounders also have better horizontal resolution than UV-VIS sounders determined by the IFOV size and pixel spacing. Since infrared instruments are not dependent on the atmosphere being sunlit to obtain measurements, they are also able to sample the atmosphere with twice the temporal frequency obtaining measurements both during the day and at night.

[9] The detection limit for the SO_2 total column for the current generation of both infrared and UV-VIS sensors has been quoted as 2 DU in the context of aviation hazard avoidance in Europe [*Zehner*, 2010]. The detection limit for volcanic SO_2 from the IASI instrument itself is currently estimated at 2 DU [*Clerbaux et al.*, 2009]. This presents difficulties for the detection of events similar to Eyjafjallajökull as the amount of SO_2 present during the initial stages of the explosive phase was too low and at too low an altitude to be detected reliably using existing systems. The continuing eruption was not highlighted by the SACS SO_2 alert system until 21 April 2010, and significant levels of SO_2 were difficult to discern using current near-real-time methods from IASI until 5 May 2010 after the start of a more SO_2 rich phase.

[10] Figure 1 shows the plume of SO_2 from Eyjafjallajökull on the morning of 15 April 2010, which is the first time the UV instruments could see the plume. At this stage, the column amounts reported in the near-real-time retrievals from the instruments in SACS did not exceed 2 DU. Even though the plume of SO_2 extending south-east from Iceland can be discerned manually in both the OMI and GOME-2 near-real-time data, there are artifacts elsewhere not related to the plume which are of a similar magnitude and make the volcanic plume difficult to discriminate from surrounding measurements. The plume was also observed using the BTD method from IASI, but as can be seen from Figure 2, the SO_2 signal is close to the noise level. Unlike the UV instruments, IASI was also able to view the atmosphere shortly after the start of the explosive phase on the evening of 14 April during darkness hours. Here, the amount of SO_2 was even lower and the geographical extent of the plume was still very limited which made detection difficult at this point. It is likely that the detection of the start of the explosive phase from space was not possible using currently implemented methods.

[11] The IASI instrument was launched aboard the EUMETSAT MetOp-A platform in October 2006. It is a

Figure 1. The Eyjafjallajökull event on the morning of 15 April 2010 as observed using OMI, GOME-2 and SCIAMACHY near-real-time total column SO_2 retrievals as implemented in the Support to Aviation Control Service (SACS). These plots have been reproduced with permission from the SACS Web site (http://sacs.aeronomie.be/nrt/index_NRT.php?Year=2010&Month=04&Day=15&InstruGOME2=1&InstruOMI=2&InstruSCIA=3&InstruIASI=4&InstruAIRS=5&obsVCD=1&obsAAI=0&obsCCF=0&modeONE=0&modeADD=1&horaireIASI=1&horaireAIRS=1&Region=106). The SACS is financed by the European Space Agency, project managed by BIRA-IASB in collaboration with KNMI, ULB and DLR.

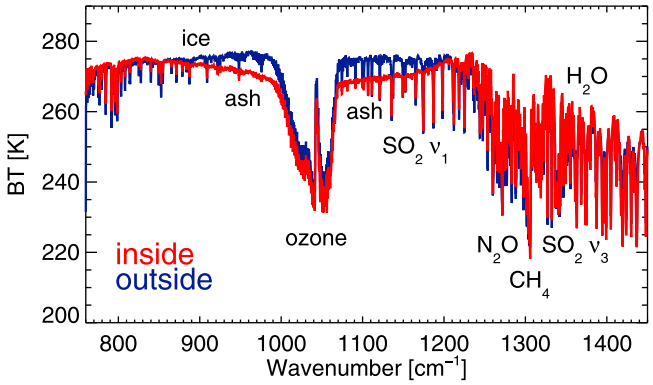

Figure 3. Comparison of real spectra obtained inside and outside of the plume from Eyjafjallajökull on 15 April 2010. Spectrum inside the plume shown in red was obtained at 10.48 UTC at [lon, lat] = [1.303°, 61.566°]. Spectrum outside the plume shown in blue was obtained at 10.54 UTC at [lon, lat] = [−2.202°, 39.010°].

high spectral resolution nadir-viewing Fourier transform spectrometer operating in the thermal infrared with continuous spectral coverage between 645–2760 cm^{-1} sampled at a spectral resolution of 0.25 cm^{-1}. The footprint of the instrument consists of four circular IFOV's each with a radius of 12.3 km in the near nadir which are scanned in the cross-track direction resulting in a swath width of ~2200 km. The instrument is in a sun-synchronous orbit with global coverage providing a morning and evening measurement each day at a given location. The instrument is used for operational measurements of meteorological parameters for numerical weather prediction. However, the high density of spectral information available and good signal-to-noise characteristics mean that the instrument can also provide measurements of many chemical species. Full retrievals are time-consuming when searching for a sporadic event such as a volcanic eruption within a large data set. Detection methods do not require on-line radiative transfer calculations and can therefore be used to provide atmospheric measurements quickly, for example to help with volcanic hazard avoidance. Calibration methods can then be used to link the observed BTD to total column amounts to provide more quantitative information [*Clarisse et al.*, 2008; *Karagulian et al.*, 2010].

[12] Some idea of the sensitivity required to detect SO_2 in the initial phases of the Eyjafjallajökull eruption is given by Figure 3, which shows examples of real IASI spectra from inside and outside of the plume from Eyjafjallajökull on the morning of 15 April 2010. The characteristic "V" shape distortion of the spectrum due to volcanic ash in the region 800–1215 cm^{-1} is visible in the spectrum originating from the plume. In the spectrum outside of the plume, there is curvature in the opposite sense below around 1000 cm^{-1} due to ice cloud. In both spectra, there are strong absorption bands due to ozone and water vapor. Unlike more SO_2 rich eruptions, the spectral signature of SO_2 is difficult to manually detect in the spectrum from inside the plume, especially the SO_2 ν_3 band centered on 1362 cm^{-1} which is entirely obscured by much greater absorption due to water vapor. For automatic detection of the SO_2 signal, the main difficulty is accounting for the variability of parameters such as water vapor and ice and water cloud, which is much greater than the SO_2 signal for weak volcanic eruptions.

[13] It is possible to discriminate the SO_2 signal by exploiting the large amount of spectral information available from IASI. The high density of spectral information and low instrument noise means that IASI could potentially provide very sensitive detections of SO_2, especially for plumes in the upper-troposphere and lower-stratosphere, where the thermal contrast with the layers below is maximized. In clean-air conditions, total SO_2 column amounts of less than 0.2 DU concentrated in the boundary layer between 0–2 km are typical [*Eisinger and Burrows*, 1998], and in this case simulations show that the signal falls well below the noise level of the instrument. However, when SO_2 is injected much higher into the atmosphere by an explosive volcanic event it may be possible to discern very low concentrations. As shown in Figure 4, there are two SO_2 bands in the thermal infrared: the symmetric stretch ν_1 band centered on 1152 cm^{-1} and the antisymmetric stretch ν_3 band centered on 1362 cm^{-1}. Figure 4 shows the simulated absorption due to a 0.1, 0.3, 1.0, 2.0, and 5.0 DU plume of SO_2 between the altitudes of 9 and 10 km. When only a handful of channels are used to sense SO_2 then a detection limit of 2 DU appears reasonable in the ν_3 band according to Figure 4. However, the limitation due to instrument noise can be reduced by combining many channels. The problem then consists of isolating the contribution of SO_2 whilst suppressing unwanted contributions from other parameters affecting the measurement such as water vapor and clouds.

2. Methodology

[14] A fast method to detect SO_2 is described which uses many spectral channels to separate the contribution of SO_2 from the contribution of other parameters affecting the measurement. All spectral modeling was performed using the Reference Forward Model (RFM) which is a line-by-line radiative transfer code, including the HITRAN-2008 spectral database [*Rothman et al.*, 2009]. Details about the RFM can be found in the online manual (http://www.atm.ox.ac.uk/RFM). A viewing angle correction was applied to the spectra to account for the greater path length traveled through the atmosphere in the off-nadir views. The spectra were scaled by an air mass factor $\cos(\phi)$ where ϕ is the satellite zenith angle.

[15] It is assumed that the spectral measurements $\mathbf{y} \in \mathbb{R}^m$ can be represented by the forward model F plus the total measurement error

$$\mathbf{y} = F(x_c,\ \mathbf{u}) + \boldsymbol{\epsilon}_{\mathrm{rnd}} + \boldsymbol{\epsilon}_{\mathrm{sys}} \tag{1}$$

where x_c is the total column amount of SO_2, $\mathbf{u}$ represents the best estimate of other parameters related to the atmosphere, surface, and instrument, $\boldsymbol{\epsilon}_{\mathrm{rnd}}$ is the random measurement error determined by instrument noise, and $\boldsymbol{\epsilon}_{\mathrm{sys}}$ represents systematic measurement errors due to uncertainties in parameters $\mathbf{u}$. The forward model is linearized about a reference state with climatological levels of the target gas and our best knowledge of the parameters $\mathbf{u}$ where the detection is

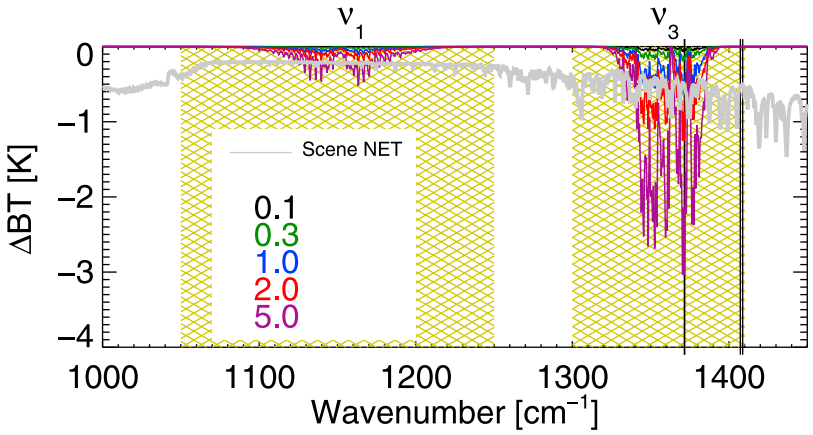

Figure 4. Signal from SO_2 in the thermal infrared for a 0.1, 0.3, 1.0, 2.0, and 5.0 DU plume between 9 and 10 km. The contribution to signal from SO_2 was calculated as the observed brightness temperature with the SO_2 layer in an otherwise standard atmosphere minus the observed brightness temperature of a standard atmosphere without the SO_2 layer. The silver line shows the Noise Equivalent Temperature (NET) for a typical scene. Vertical lines show the positions of the four channels used in the flag for SO_2 from IASI by *Clarisse et al.* [2008]. The yellow cross-hatched area shows the channels used in the fast ν_1 band and ν_3 band retrievals.

applied. When the forward model is nearly linear around the climatological atmospheric conditions, we can write

$$\mathbf{y} = F(x_{c0},\ \mathbf{u}) + \mathbf{k}(x_c - x_{c0}) + \boldsymbol{\epsilon}_{\text{rnd}} + \boldsymbol{\epsilon}_{\text{sys}} \tag{2}$$

where x_{c0} is the linearization point taken to be a climatological value of the SO_2 total column, and the i-th row of the Jacobian $\mathbf{k} \in \mathbb{R}^m$ can be written as $\frac{\partial y_i}{\partial x_c}$ where y_i are in brightness temperature. Let us now consider an ensemble of spectral measurements with unbiased errors with enough members to capture the climatological variability of the atmosphere in the absence of a volcanic event. If the mean of the ensemble of $\mathbf{y}$ is denoted as $\bar{\mathbf{y}}$, from equation (2) we can write

$$\bar{\mathbf{y}} = F(x_{c0},\ \mathbf{u}) + \mathbf{k}(\bar{x}_c - x_{c0}) + \bar{\boldsymbol{\epsilon}}_{rnd} + \bar{\boldsymbol{\epsilon}}_{sys} = F(x_{c0},\ \mathbf{u}) \tag{3}$$

where $\bar{x}_c \equiv x_{c0}$. We then perform a fast one-step retrieval of the SO_2 total column amount. From *Rodgers* [2000] and equation (3), the optimal least-squares estimate is given by

$$\begin{aligned} \hat{x}_c &= x_{c0} + \left(\mathbf{k}^T \mathbf{S}_{\boldsymbol{\epsilon}}{}^{-1} \mathbf{k}\right)^{-1} \mathbf{k}^T \mathbf{S}_{\boldsymbol{\epsilon}}{}^{-1} (\mathbf{y} - F(x_{c0}, \mathbf{u})) \\ &= x_{c0} + \mathbf{g}^T (\mathbf{y} - F(x_{c0}, \mathbf{u})) \\ &= x_{c0} + \mathbf{g}^T (\mathbf{y} - \bar{\mathbf{y}}) \end{aligned} \tag{4}$$

where $\mathbf{g}^T \in \mathbb{R}^{1\times m}$ is the retrieval gain, and the total measurement error covariance $\mathbf{S}_\epsilon \in \mathbb{R}^{\mathrm{m}\times\mathrm{m}}$ is the covariance of the total error $(\boldsymbol{\epsilon}^{\text{rnd}} + \boldsymbol{\epsilon}^{\text{sys}})$ where $\boldsymbol{\epsilon}^{\text{rnd}}$ is the random measurement error due to instrument noise and $\boldsymbol{\epsilon}^{\text{sys}}$ are systematic measurement errors due to variability in parameters other than SO_2 such as cloudiness, atmospheric temperature and surface temperature, and interfering species such as water vapor. The systematic errors tend to be spectrally correlated. These long-range correlations in the total measurement error covariance fix the spectral baseline against which the presence of SO_2 is determined. This achieves a similar effect to a standard joint retrieval of all parameters affecting the measurement [*von Clarmann et al.*, 2001]. The total measurement error covariance can be estimated by using an appropriate ensemble of real spectra, in which case the real variability in the physical radiative transfer process due variability in the atmospheric state becomes part of the measurement noise. This greatly simplifies the problem of retrieving SO_2 as it removes the need to quantify interference from other species and clouds, which is a major task using standard retrieval methods. The same inversion can be used on any spectral measurement regardless of the concentration of water vapor, surface temperature, and conditions of cloudiness and any other variables which have an impact on the retrieval, as long as these parameters are within the variability sampled by the ensemble used to create the total measurement error covariance. No special treatment is then needed for cloudy scenes, for example, and SO_2 can be detected above cloud layers provided that the thermal contrast between the SO_2 layer and the cloud is sufficiently large.

[16] The mean spectrum $\bar{\mathbf{y}}$ and the total measurement error covariance $\mathbf{S}_\epsilon$ were computed using an appropriate ensemble of measured spectra. The ensemble used consists of 196,042 measured spectra acquired during April of the previous year (2009) where no enhancements in SO_2 were expected in the latitude box bounded by the [lon, lat] coordinates [−40,30] and [10, 70]. It was assumed that this ensemble adequately captures the variability of the atmosphere at the same time of year and location in 2010. The mean spectrum for the background atmosphere $\bar{\mathbf{y}}$ is given by

$$\bar{\mathbf{y}} = \frac{1}{N} \sum_{j=1}^{N} \mathbf{y}_j \tag{5}$$

where N are the number of spectra in the ensemble. The total measurement error covariance $\mathbf{S}_\epsilon \in \mathbb{R}^{m\times m}$ is computed

$$\mathbf{S}_{\mathbf{y}} \equiv \frac{1}{\mathbf{N}-1} \sum_{\mathbf{j}=1}^{\mathbf{N}} \left(\mathbf{y_j} - \bar{\mathbf{y}}\right) \left(\mathbf{y_j} - \bar{\mathbf{y}}\right)^{\mathbf{T}} \simeq \mathbf{S}_\epsilon \tag{6}$$

This method to calculate the total measurement error covariance assumes that background levels of SO_2 in clean air are low enough to generate a signal well below the noise level of the instrument so that $\mathbf{S_y} \backsimeq \mathbf{S}_\epsilon$. This is reasonable for SO_2 since calculations (not shown) indicate that the signal from levels of SO_2 in the absence of volcanic emissions is an order of magnitude below the instrumental noise.

[17] Once a suitable ensemble has been defined, and $\bar{\mathbf{y}}$ and $\mathbf{S}_\epsilon$ have been estimated, it is straightforward to calculate the retrieval gain $\mathbf{g}^T$, see equation (4). The retrieval gain is the vector of coefficients which are applied to the incoming spectra to determine the presence of SO_2. In principle, a single globally applicable vector of coefficients can be used to detect SO_2 by using an ensemble which samples all seasons and locations. In practice, however, a more sensitive detection of SO_2 can be obtained by using a vector which is specific to a particular geographical region and time of year to target a particular group of volcanoes in a given season. This is the approach we have adopted for the Eyjafjallajökull event, defining a vector of coefficients suitable for Europe and the North Atlantic in the month of April. Once this vector has been defined, the method is straightforward to apply operationally since the detection of SO_2 only requires the multiplication of the incoming spectra by a single vector of coefficients. The method is therefore equivalent in computational speed to existing brightness temperature difference techniques [e.g., *Clarisse et al.*, 2008] but has the advantage of using many more channels to maximize sensitivity.

[18] Two separate retrievals were performed: one using the ν_1 band and one using the ν_3 band. All channels in each SO_2 absorption band were used as shown in Figure 4. The ν_3 band retrieval was performed using channels between 1300–1410 cm^{-1} (441 channels). Here there is very limited sensitivity to the lower troposphere due to strong interference from water vapor. The ν_1 band retrieval was performed using channels between 1050–1250 cm^{-1} (801 channels). One complication in this spectral region is that the ν_1 band overlaps a spectral signature due to volcanic ash which can obscure the signal from SO_2. In addition, there are sharp spectral features due to strong reflections from the quartz Reststrahlung band between 1100–1250 cm^{-1} (E. Pavelin, personal communication, 2009). However, if the ensemble adequately samples these spectral features then they effectively become part of the measurement noise. This does not therefore preclude the use of the ν_1 band over desert surfaces as long as the ensemble used to generate the total measurement error covariance includes these regions.

[19] A suitable detection threshold may be defined by considering the estimated standard deviation on the SO_2 total column amount

$$\hat{\sigma}_c = \left(\mathbf{k}^T \mathbf{S}_\epsilon{}^{-1} \mathbf{k}\right)^{-\frac{1}{2}} \tag{7}$$

For background atmospheric conditions, the retrieved values of SO_2 are well approximated by a Gaussian distribution which is centered on the background atmospheric concentration of SO_2, x_{c0}, with a standard deviation given by equation (7). Given the standard deviation of this distribution, a value can be defined for which there is a very low probability that a measurement of SO_2 exceeding this value is due to fluctuations arising from measurement noise or climatological variations in the background atmospheric state. Since the IASI instrument acquires approximately 1.3 million spectra each day, a strict detection threshold is needed. A retrieved value of SO_2 which is 5.1993 $\hat{\sigma}_c$ greater than the concentration in the background atmosphere has just a one in 10 million chance of being due to variability arising from measurement noise and variations in the background atmospheric state. This was therefore chosen as a suitable criterion for the detection threshold. In the context of an automated detection, this could be combined with a cluster test to look for structures which are likely to correspond to a volcanic plume. Hence, a positive detection of SO_2 is defined as

$$\hat{x}_c > x_{c0} + 5.1993\hat{\sigma}_c \tag{8}$$

This can be used as the basic criterion for the detection of a significant level of SO_2 present in the levels of the atmosphere to which the instrument is sensitive. Further details about the method described above is provided by *Walker et al.* [2011].

3. Observations of the Plume of Sulphur Dioxide From Eyjafjallajökull

[20] The plume of SO_2 is observed using IASI during the initial stages of the explosive phase on the 14 and 15 of April 2010. Figure 5 shows the plume of SO_2 from Eyjafjallajökull as observed on the nighttime overpass on 14 April 2010 for the first available observations from IASI after the start of the explosive phase. There is no plume of SO_2 apparent using the BTD filter or the ν_1 band. However, in Figure 5c a small plume of SO_2 can be discerned close to the volcano on the south coast of Iceland using the ν_3 band. Figure 6 shows the distribution of observed values for each method as histograms. Values exceeding the detection threshold in the histogram are highlighted as asterisks. No values are above the detection threshold using the BTD filter. There are some values above the detection threshold associated with the plume using the ν_1 band but most of these are associated with surface emissivity features over desert in North Africa. Using the ν_3 band, there are 9 observations associated with the volcanic plume and no false detections out of almost 9000 observations in the scene. The geographical extent of the plume is still limited at this stage. A close-up of the volcanic plume observed on the evening of the 14 April is shown in Figure 7 before and after the application of the detection threshold. There are no false positives in the scene, and the plume is clearly discerned, given the strict detection criterion that has been applied, equation (8). This means that it was possible to detect the very early stages of the explosive phase of this eruption from space using the first available IASI data.

[21] Figure 8 shows SO_2 as observed on the morning of 15 April corresponding to Figures 1 and 2 which show the plume observed by the sensors in the SACS alert system using near-real-time retrieval methods. By this stage, the plume had drifted south-east from Iceland extending towards Scandinavia. In this case, it is possible to make out the SO_2 plume by eye using both the BTD filter and ν_1 band but the observations are close to the noise level for the scene.

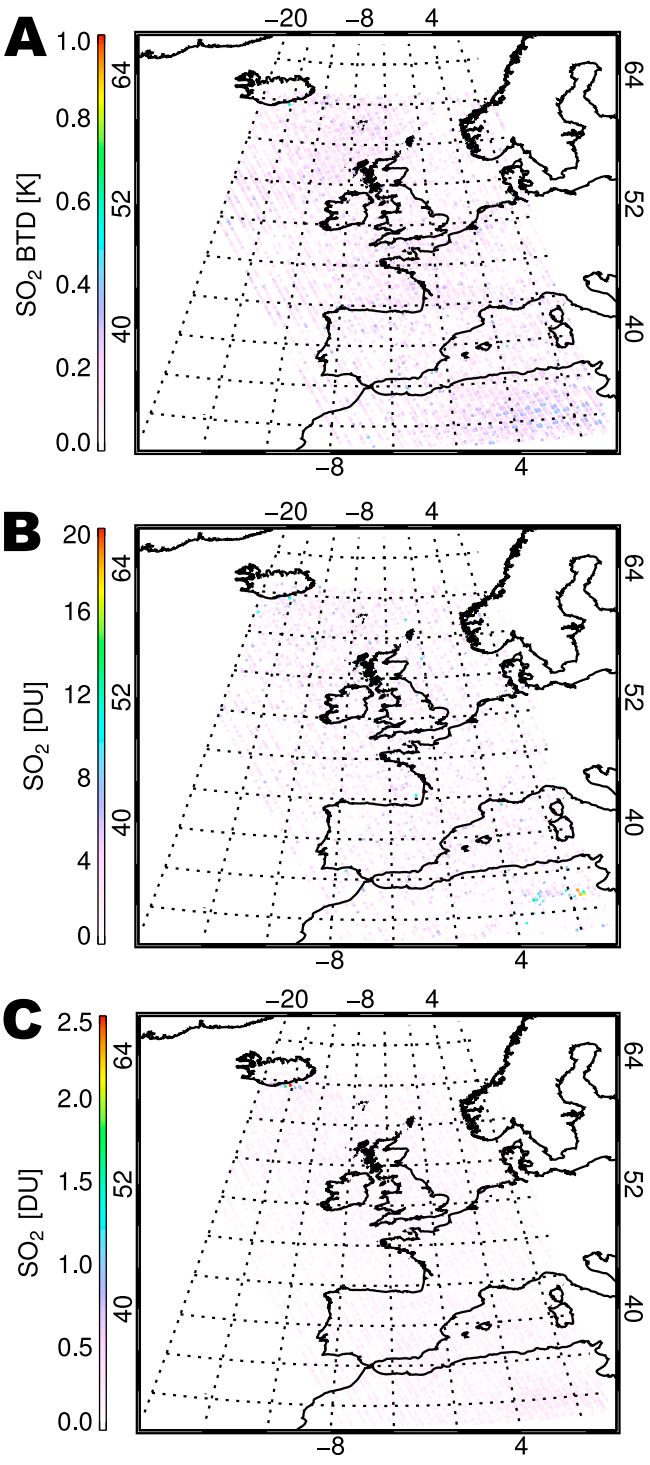

Figure 5. The plume of SO_2 from Eyjafjallajökull as observed on the evening of 14 April 2010 at 21.03 UTC. (a) The brightness temperature difference between SO_2 sensitive and background channels using the four-channel method. (b) The estimated total SO_2 column using the ν_1 band fast retrieval. (c) The estimated total SO_2 column using the ν_3 band fast retrieval. Elevated levels of SO_2 are just visible close to the volcano on the south coast of Iceland in Figure 5c using the ν_3 band.

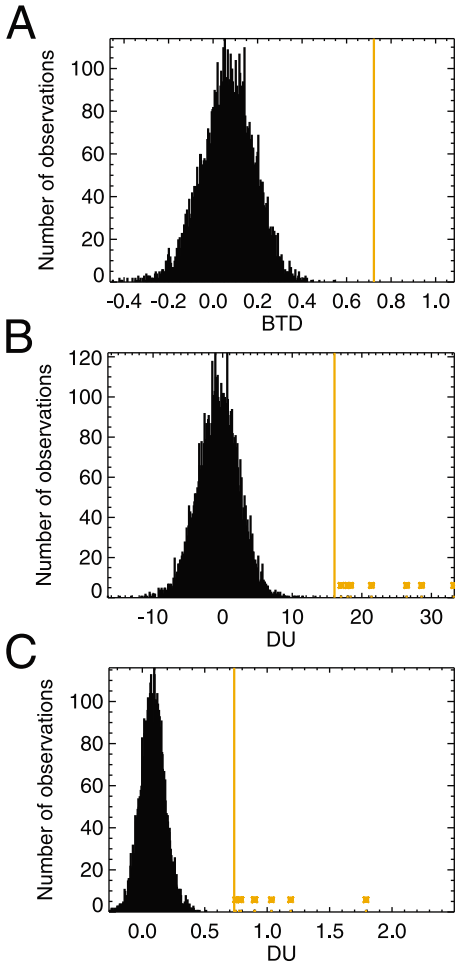

Figure 6. Distribution of SO_2 values for entire scene shown in Figure 5 for evening overpass on 14 April observed using: (a) BTD filter, (b) ν_1 band retrieval, and (c) ν_3 band retrieval. The orange line shows the detection threshold given by equation (8). Measurements exceeding the detection threshold are shown as orange asterisks.

However, using the ν_3 band fast retrieval, the noise level is much lower and the plume is clearly distinguished. To examine how well the plume has been detected in this case, the distribution of values for each method is shown in Figure 9 as histograms and the detection threshold is indicated. Inspecting the values, two IFOV close to the volcano are above the detection threshold for the BTD filter but there are other higher BTD values in the scene distant from the volcano which mean that in practice a higher threshold needs to be used. Using the ν_1 band, there are 11 values identified as belonging to the plume and the problem area over desert is avoided in this case. Using the ν_3 band, however, there are 118 values above the detection threshold and no false detections anywhere in the scene out of almost 9000 measurements. A close-up of the plume using the fast ν_3 band retrieval is shown in Figure 10 before and after the application of the detection threshold. The plume on the morning of 15 April is easily detectable from IASI using this method.

[22] An estimate of the detection limit for volcanic plumes of SO_2 using IASI was calculated. For measurements in the

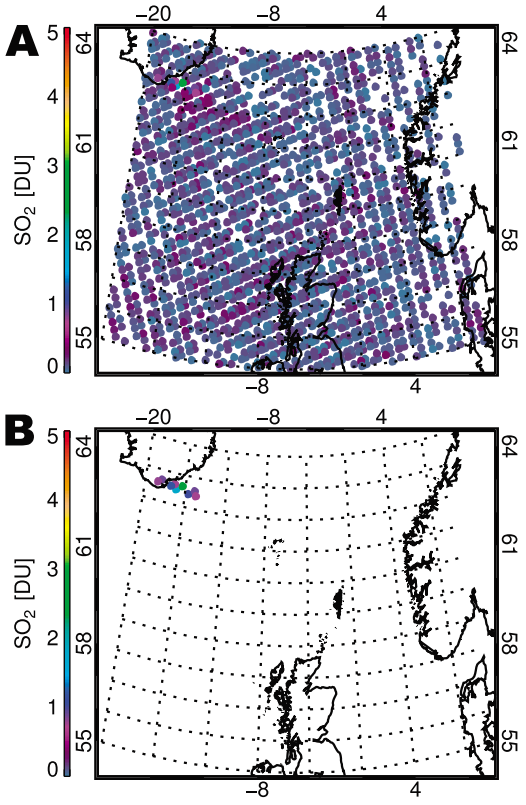

Figure 7. The volcanic plume detected by IASI using the fast ν_3 band retrieval on the evening of 14 April 2010 after the application of the detection threshold given by equation (8). (a) The value of the plume and the surrounding background values. (b) The plume after the application of the detection threshold.

thermal infrared, the sensitivity is better for plumes injected higher in the troposphere where the atmosphere is colder and there is higher thermal contrast with the underlying layers. Conversely, for plumes lower in the troposphere the lower thermal contrast means sensitivity to SO_2 is lower. The most sensitive measurements of SO_2 can be obtained when the plume sits at the tropopause cold-point which is often reached or surpassed in larger explosive events. As the SO_2 signal is dependent on thermal contrast, different assumptions about the vertical distribution of SO_2 in the fast retrieval change the Jacobian **k** which changes the retrieved total column amount, see equation (4). The fast retrieval is therefore a qualitative method as it depends on the assumed altitude distribution of the plume. A more quantitative estimate of the total column can be provided when an external estimate of the plume altitude is available, or the values retrieved can be calibrated directly against a fully quantitative retrieval. The effect of assumed plume altitude in the fast retrieval using the ν_3 band is shown in Figure 11. The total column amount of SO_2 calculated in the plume for the evening overpass of 15 April in Figure 10, computed assuming a climatological vertical distribution, is compared against the values which would have been retrieved in the ν_3 spectral region assuming instead that the SO_2 plume is confined to altitudes of 0–2 km, 2–4 km, 4–6 km, 6–8 km,

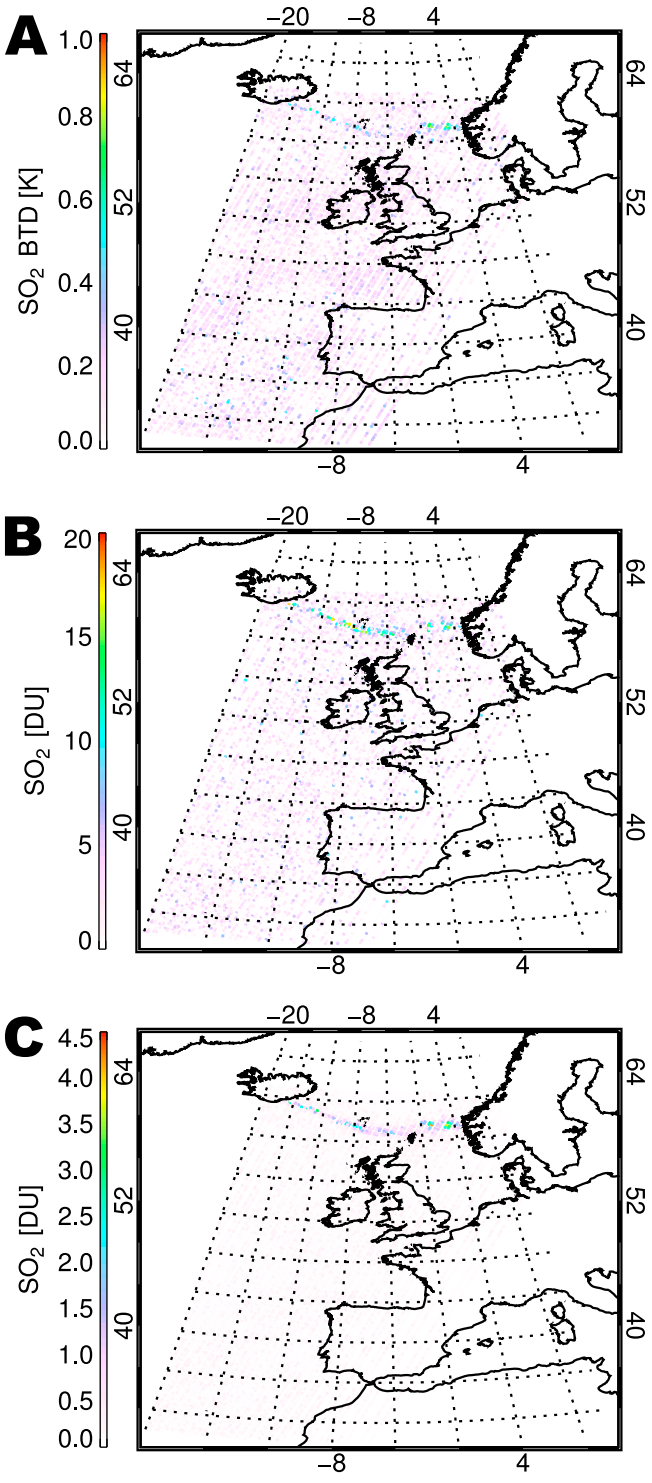

Figure 8. The plume of SO_2 from Eyjafjallajökull as observed on the evening of 15 April 2010 at 10.48 UTC. (a) The brightness temperature difference between SO_2 sensitive and background channels using the four-channel method. (b) The estimated total SO_2 column using the ν_1 band fast retrieval. (c) The estimated total SO_2 column using the ν_3 band fast retrieval.

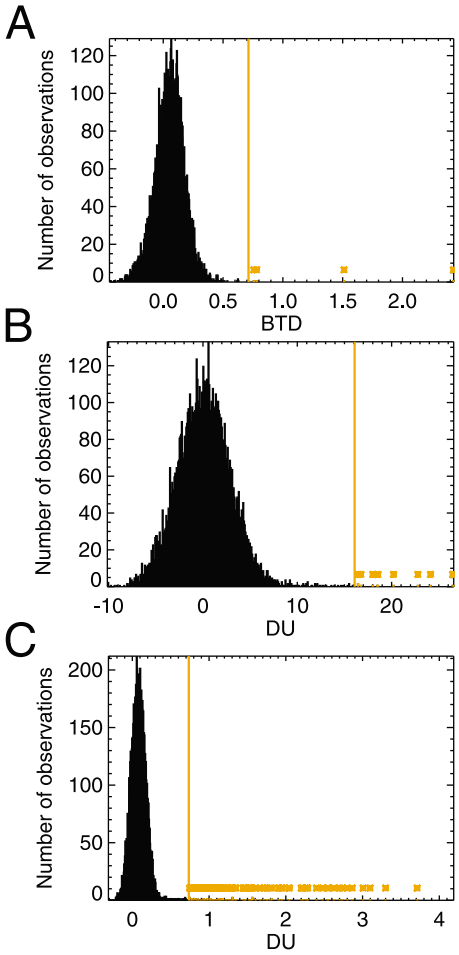

Figure 9. Distribution of SO_2 values for entire scene shown in Figure 8 for the morning overpass on 15 April 10.48 UTC observed using: (a) BTD filter, (b) ν_1 band retrieval, and (c) ν_3 band retrieval. The orange line shows the detection threshold given by equation (8). Measurements exceeding the detection threshold are highlighted as asterisks.

8–11 km, 11–14 km, and 14–18 km where all altitudes refer to the height above sea level. When the plume is confined to the boundary layer between 0–2 km the fast retrieval assigns much larger total column SO_2 to the observations due to strong shielding of the low altitude SO_2 signal by optically thick water vapor lines in the ν_3 region (Figure 11). For a plume confined between 2–4 km the estimated total column amount is approximately a factor 5 higher, for a plume between 4–6 km it is approximately a factor 2 higher, for a plume between 6–8 km it is almost the same, for a plume between 8–11 km it is approximately a factor 2 lower, for a plume between 11–14 km it is a factor 2.4 lower, and for a plume between 14–18 km it is approximately a factor 3 lower. To estimate the detection limit of the instrument, we can use the slopes of the best fit lines shown in Figure 11 to scale the detection threshold in equation (8) for plumes at different levels in the atmosphere. The results are shown in Table 1. The sensitivity to SO_2 in the boundary layer is low at 17.0 DU due to strong interference from optically thick water vapor lines. However, the instrument is sensitive to very low amounts of SO_2 higher in the atmosphere and using the conservative detection threshold in equation (8), the detection limit calculated at the tropopause cold-point is estimated as 0.3 DU. This implies that the detection limit using IASI is an order of magnitude better than previously thought [*Clerbaux et al.*, 2009; *Zehner*, 2010].

[23] An estimate was then derived for the detection limit for the plume from Eyjafjallajökull on 15 April. Figure 12 compares the fast SO_2 retrieval against a fully quantitative optimal estimation type retrieval of SO_2 and plume altitude (E. Carboni et al., A new retrieval scheme for SO_2 from IASI measurements: Application to the Eyjafjallajökull eruption during April and May 2010, manuscript in preparation, 2012). The retrieval assumes a Gaussian distribution for the vertical SO_2 profile and returns the SO_2 column amount and the altitude of the plume. Radiative transfer computations that generate the forward modeled spectra (against which the measurements are compared) are based on RTTOV [*Saunders et al.*, 1999] and ECMWF meteorological data. The retrieval is based on an optimal estimation scheme and includes a comprehensive error budget for every pixel. This is derived from an error covariance matrix that is based on the SO_2-free climatology of the difference between the IASI and forward model spectra. The full retrieval uses both the SO_2 ν_1 band using channels between 1000–1200 cm^{-1}

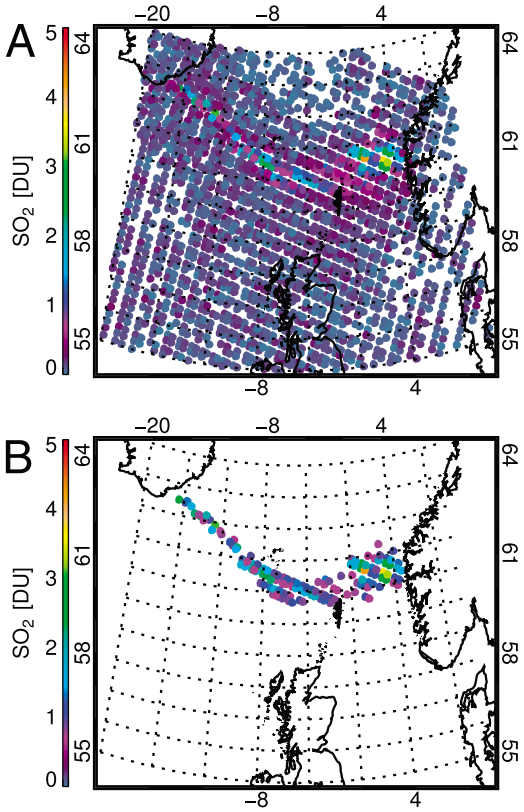

Figure 10. The volcanic plume detected by IASI using the fast ν_3 band retrieval on the morning of 15 April 2010 after the application of the detection threshold given by equation (8). (a) The value of the plume and the surrounding background values. (b) The plume after the application of the detection threshold.

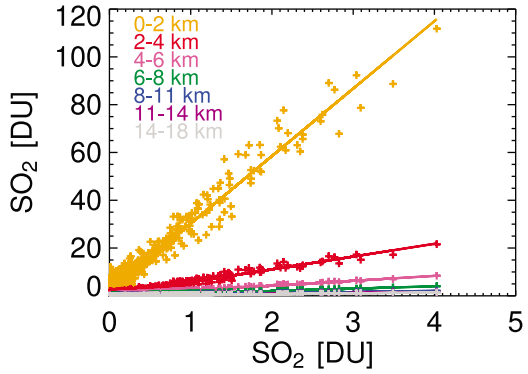

Figure 11. Plotted points correspond to values retrieved using the ν_3 band fast retrieval with different assumptions about the plume altitude for the morning overpass on 15 April for the plume shown in Figure 10. The horizontal axis shows the SO_2 column observed using the ν_3 band fast retrieval assuming a climatological vertical distribution. The vertical axis shows the total column amounts for SO_2 which would have been obtained using a different assumption about the vertical distribution of SO_2 where orange corresponds to a plume confined to 0–2 km (slope of best fit = 28.0), red 2–4 km (slope = 5.3), fuchsia 4–6 km (slope = 2.1), green 6–8 km (slope = 1.0), blue 8–11 km (slope = 0.54), purple 11–14 km (slope = 0.42), and silver to 14–18 km (slope = 0.38).

as well as the ν_3 band using channels between 1300–1410 cm^{-1}. Information about the altitude of the plume is contained in the different spectral signatures of SO_2 and water vapor in the ν_3 band.

[24] The plume height in the full retrieval is mostly between 2–6 km. There are 7 points with retrieved altitudes of 0–2 km, 141 points at 2–4 km, 32 points at 4–6 km, and 2 points at 6–8 km. In the fast SO_2 retrieval, when the plume height is assumed to be within 0–2 km the retrieved values are mostly higher than in the full retrieval. Conversely, when the plume altitude is assumed to be 6–8 km in the fast SO_2 retrieval, the values are lower than in the full retrieval, illustrating the dependence on assumed altitude distribution in the fast retrieval in common with other near-real-time methods. When the plume is assumed to lie at 2–4 km and 4–6 km the best agreement is obtained. The retrieved heights in the full retrieval appear reasonable considering ground-based lidar observations and the UK

Table 1. The Detection Threshold (x_{c0} + 5.1993 $\hat{\sigma}_c$ DU) for SO_2 Plumes at Various Altitudes Using the ν_3 Band Fast Retrieval

Altitude (km)	x_{c0} + 5.1993 $\hat{\sigma}_c$ (DU)
0–2	17.0
2–4	3.3
4–6	1.3
6–8	0.7
8–11	0.40
11–14	0.33
14–18	0.30

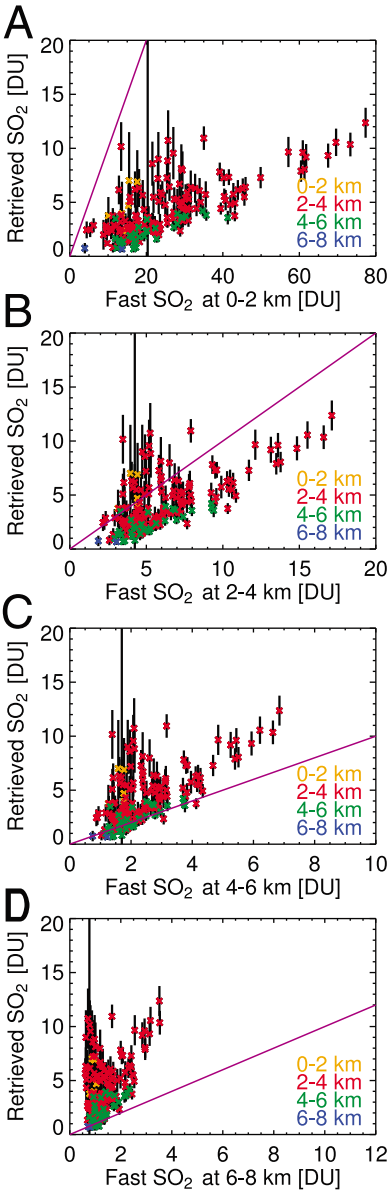

Figure 12. The SO_2 total column obtained using the ν_3 band fast retrieval with different assumptions about the vertical distribution of SO_2 is compared against a fully quantitative retrieval of SO_2 total column amount and plume altitude. The full SO_2 retrieval is compared against the fast SO_2 retrieval where the plume is (a) confined to 0–2 km in the fast retrieval, (b) confined to 2–4 km in the fast retrieval, (c) confined to 4–6 km in the fast retrieval, and (d) confined to 6–8 km in the fast retrieval. The legend indicates the altitude retrieved in the fully quantitative retrieval. The purple line indicates $x = y$.

Met Office's NAME estimates of the altitude of the transported ash plume during the initial phase of the eruption [*Dacre et al.*, 2011]. Hence, assuming a plume altitude in the fast SO_2 retrieval of 2–4 km and using the slopes in Figure 11 to scale the detection threshold calculated using equations (7) and (8) accordingly, the sensitivity with which

the plume of SO_2 could be detected on the morning of 15 April using a conservative criterion is 3.3 DU.

4. Conclusions

[25] The plume of SO_2 from the eruption of the Eyjafjallajökull volcano in Iceland was observed using the MetOp-A IASI instrument for the start of the explosive phase on 14–15 April 2010. The amount of SO_2 contained in the plume was initially low and was not detected by current satellite-based alert systems. The potential of IASI to provide highly sensitive measurements of volcanic SO_2 was examined for the initial phase of the eruption using a fast retrieval of SO_2 which exploits the hyperspectral nature of the sensor. The plume was positively identified using the ν_3 band absorption feature using a conservative detection threshold on the evening of 14 April. The plume could also easily be discerned on the morning of the 15 April when it had drifted south-east towards Scandinavia. The relationship between the sensitivity of the fast retrieval for different assumed vertical distributions of SO_2 was then used to provide general estimates of the detection limit from the surface to the tropopause cold-point. It was estimated that the detection limit for IASI is 0.3 DU for a plume at the tropopause cold-point using a conservative detection threshold. This is an order of magnitude lower than previously thought [*Clerbaux et al.*, 2009; *Zehner*, 2010]. A fully quantitative optimal estimation type retrieval of total column SO_2 and plume altitude was applied to the data from the morning overpass of 15 April to calibrate the fast SO_2 retrieval. It was estimated that the detection limit for IASI for the plume at 2–4 km altitude on the 15 April was 3.3 DU. The method is fast and easy to apply and could be used to help with operational monitoring of SO_2 for aviation hazard avoidance.

[26] **Acknowledgments.** This work was funded by the UK Natural Environment Research Council (NERC) National Centre for Earth Observation (NCEO) Atmospheric Composition and Dynamic Earth and Geohazards Themes. Thanks go to the three anonymous reviewers for their comments. Thanks go to Stefano Migliorini for his comments.

References

Carn, S., A. Krueger, N. Krotkov, K. Yang, and K. Evans (2009), Tracking volcanic sulfur dioxide clouds for aviation hazard mitigation, *Nat. Hazards*, *51*(2), 325–343, doi:10.1007/s11069-008-9228-4.

Casadevall, T. J., P. J. Delos Reyes, and D. J. Schneider (1996), The 1991 Pinatubo eruptions and their effect on aircraft operations, in *Fire and Mud —Eruptions and Lahars of Mount Pinatubo, Philippines*, edited by C. G. Newhall and R. S. Punongbayan, pp. 1071–1088, Univ. of Wash. Press, Seattle.

Clarisse, L., P. F. Coheur, A. J. Prata, D. Hurtmans, A. Razavi, T. Phulpin, J. Hadji-Lazaro, and C. Clerbaux (2008), Tracking and quantifying volcanic SO_2 with IASI, the September 2007 eruption at Jebel at Tair, *Atmos. Chem. Phys.*, *8*, 7723–7734.

Clarisse, L., F. Prata, J. L. Lacour, D. Hurtmans, C. Clerbaux, and P. F. Coheur (2010), A correlation method for volcanic ash detection using hyperspectral infrared measurements, *Geophys. Res. Lett.*, *37*, L19806, doi:10.1029/2010GL044828.

Clerbaux, C., et al. (2009), Monitoring of atmospheric composition using the thermal infrared IASI/MetOp sounder, *Atmos. Chem. Phys.*, *9*(16), 6041–6054, doi:10.5194/acp-9-6041-2009.

Dacre, H. F., et al. (2011), Evaluating the structure and magnitude of the ash plume during the initial phase of the 2010 Eyjafjallajökull eruption using lidar observations and NAME simulations, *J. Geophys. Res.*, *116*, D00U03, doi:10.1029/2011JD015608.

Eisinger, M., and J. P. Burrows (1998), Tropospheric sulphur dioxide observed by the ERS-2 GOME instrument, *Geophys. Res. Lett.*, *25*(22), 4177–4180.

Gudmundsson, M. T., R. Pedersen, K. Vogfjörd, B. Thorbjarnardóttir, S. Jakobsdoóttir, and M. J. Roberts (2010), Eruptions of Eyjafjallajökull Volcano, Iceland, *Eos Trans. AGU*, *91*(21), 190–191, doi:10.1029/2010EO210002.

Guffanti, M., T. J. Casadevall, and K. Budding (2010), Encounters of aircraft with volcanic ash clouds: A compilation of known incidents, 1953–2009, *U.S. Geol. Surv. Data Ser. 545, Ver 1.0*, 12 pp., U.S. Geol. Surv., Reston, Va.

International Civil Aviation Organization (ICAO) (2007), Manual on volcanic ash, radioactive material and toxic chemical clouds, 2nd ed., *Doc. 9691 AN/954*, 159 pp., Montreal, Que., Canada.

International Civil Aviation Organization (ICAO) (2010), Volcanic ash contingency plan - EUR and NAT regions, *EUR Doc. 019*, 26 pp., Montreal, Que., Canada.

Jones, A. R., D. J. Thomson, M. Hort, and B. Devenish (2007), The U.K. Met Office's next-generation atmospheric dispersion model, NAME III, in *Air Pollution Modeling and its Application XVII: Proceedings of the 27th NATO, CCMS International Technical Meeting on Air Pollution Modelling and its Application*, edited by C. Borrego and A.-L. Norman, pp. 580–589, Springer, New York.

Karagulian, F., L. Clarisse, C. Clerbaux, A. Prata, D. Hurtmans, and P. Coheur (2010), Detection of volcanic SO_2, ash, and H_2SO_4 using the Infrared Atmospheric Sounding Interferometer (IASI), *J. Geophys. Res.*, *115*, D00L02, doi:10.1029/2009JD012786.

Krotkov, N., S. Carn, A. Krueger, P. Bhartia, and K. Yang (2006), Band residual difference algorithm for retrieval of SO_2 from the Aura Ozone Monitoring Instrument (OMI), *IEEE Trans. Geosci. Remote Sens.*, *44*(5), 1259–1266.

Lee, C., A. Richter, M. Weber, and J. P. Burrows (2008), SO_2 Retrieval from SCIAMACHY using the Weighting Function DOAS (WFDOAS) technique: Comparison with standard DOAS retrieval, *Atmos. Chem. Phys.*, *8*(20), 6137–6145.

Miller, T. P., and T. J. Casadevall (2000), Volcanic ash hazards to aviation, in *Encyclopedia of Volcanoes*, edited by H. Sigurdson, pp. 915–930, Academic, San Diego, Calif.

Platt, U. (1994), Differential optical absorption spectroscopy (DOAS), in *Air Monitoring by Spectroscopic Techniques*, *Chem. Anal. Ser.*, vol. 127, pp. 27–84, John Wiley, Hoboken, N. J.

Prata, A. (2009), Satellite detection of hazardous volcanic clouds and the risk to global air traffic, *Nat. Hazards*, *51*(2), 303–324, doi:10.1007/s11069-008-9273-z.

Prata, A. J., and C. Bernado (2007), Retrieval of volcanic SO_2 column abundance from Atmospheric Infrared Sounder data, *J. Geophys. Res.*, *112*, D20204, doi:10.1029/2006JD007955.

Prata, A. J., and A. Tupper (2009), Aviation hazards from volcanoes: The state of the science, *Nat. Hazards*, *51*(2), 239–244, doi:10.1007/s11069-009-9415-y.

Rix, M., P. Valks, N. Hao, T. Erbertseder, and J. Van Geffen (2008), Monitoring of volcanic SO_2 emissions using the GOME-2 satellite instrument, paper presented at Second Workshop on Use of Remote Sensing Techniques for Monitoring Volcanoes and Seismogenic Areas, INGV, Naples, Italy.

Rodgers, C. D. (2000), *Inverse Methods for Atmospheric Sounding: Theory and Practice*, *Ser. Atmos. Oceanic Planet. Phys.*, vol. 2, World Sci., Hoboken, N. J.

Rothman, L., et al. (2009), The HITRAN 2008 molecular spectroscopic database, *J. Quant. Spectrosc. Radiat. Transfer*, *110*(9–10), 533–572, doi:10.1016/j.jqsrt.2009.02.013.

Saunders, R., M. Matricardi, and P. Brunel (1999), A fast radiative transfer model for assimilation of satellite radiance observations: RTTOV-5, *Tech. Memo. 282*, ECMWF, Reading, U. K.

Showstack, R. (2011), Iceland's Grímsvötn volcano erupts, *Eos Trans. AGU*, *92*(22), 151, doi:10.1029/2011EO220003.

Simkin, T. (1993), Terrestrial volcanism in space and time, *Annu. Rev. Earth Planet. Sci.*, *21*, 427–452.

Stohl, A., et al. (2011), Determination of time- and height-resolved volcanic ash emissions and their use for quantitative ash dispersion modeling: The 2010 Eyjafjallajökull eruption, *Atmos. Chem. Phys.*, *11*(9), 4333–4351, doi:10.5194/acp-11-4333-2011.

Theys, N., R. van der A, L. Clarisse, and P. Valks (2011), SACS development, report, Eur. Space Agency, Paris. [Available at http://sacs.aeronomie.be/Documentation/SACSdevelopment.pdf.]

Thomas, H. E., and A. J. Prata (2011), Sulphur dioxide as a volcanic ash proxy during the April–May 2010 eruption of Eyjafjallajökull Volcano, Iceland, *Atmos. Chem. Phys.*, *11*(14), 6871–6880, doi:10.5194/acp-11-6871-2011.

Thomas, H. E., and I. M. Watson (2010), Observations of volcanic emissions from space: Current and future perspectives, *Nat. Hazards*, *54*(2), 323–354, doi:10.1007/s11069-009-9471-3.

Valks, P., and D. Loyola (2008), Algorithm theoretical basis document for GOME-2 total column products of ozone, minor trace gases and cloud properties (GDP 4.2 for O3M-SAF OTO and NTO), *DLR/GOME-2/ATBD/01*, 36 pp., DLR, Oberpfaffenhofen, Germany.

van der A, R., et al. (2010), GMES service element promote 2, S3 service prospectus, ver. 3, report, 55 pp., Eur. Space Agency, Paris.

van Geffen, J., M. Van Roozendael, J. van Gent, P. Valks, R. Rix, M. van der A, P. Coheur, L. Clarisse, and C. Clerbaux (2009), An alert system for volcanic SO_2 emissions using satellite measurements, paper presented at Eumetsat Meterological Satellite Conference, Eumetsat, Bath, U. K.

von Clarmann, T., U. Grabowski, and M. Kiefer (2001), On the role of non-random errors in inverse problems in radiative transfer and other applications, *J. Quant. Spectrosc. Radiat. Transfer*, *71*(1), 39–46.

Walker, J. C., A. Dudhia, and E. Carboni (2011), An effective method for the detection of trace species from MetOp IASI, *Atmos. Meas. Tech.*, *4*, 1567–1580, doi:10.5194/amt-4-1567-2011.

Witham, C. S., M. C. Hort, R. Potts, R. Servranckx, P. Husson, and F. Bonnardot (2007), Comparison of VAAC atmospheric dispersion models using the 1 November 2004 Grímsvötn eruption, *Meteorol. Appl.*, *14*(1), 27–38, doi:10.1002/met.3.

Zehner, C. (Ed.) (2010), *Monitoring Volcanic Ash From Space: Proceedings of the ESA-EUMETSAT Workshop on the 14 April to 23 May 2010 Eruption at the Eyjafjöll Volcano, South Iceland, 26–27 May 2010*, edited by C. Zehner, 110 pp., Eur. Space Agency, Paris, doi:10.5270/atmch-10-01.

E. Carboni, A. Dudhia, R. G. Grainger, and J. C. Walker, Atmospheric, Oceanic and Planetary Physics, Clarendon Laboratory, University of Oxford, Parks Road, Oxford, OX1 3PU, UK. (elisa@atm.ox.ac.uk; dudhia@atm.ox.ac.uk; grainger@atm.ox.ac.uk; walker@atm.ox.ac.uk)